



ORIGINAL ARTICLE

Synthesis of the ZnO-Ni_{0.5}Zn_{0.5}Fe₂O₄-Fe₂O₃ magnetic catalyst in pilot-scale by combustion reaction and its application on the biodiesel production process from oil residual



A.L. da Silva^{a,*}, A.F.F. Farias^a, J.R.M. Pontes^a, A.M. Rodrigues^b,
A.C.F. de M. Costa^{a,b}

^a Synthesis of Ceramic Materials Laboratory (LabSMaC), Postgraduate Program in Materials Science and Engineering (PPG-CEMat), Academic Unit of Materials Engineering, Federal University of Campina Grande, Av. Aprígio Veloso – 882, Bodocongó 58429-900, Campina Grande, PB, Brazil

^b Academic Unit of Materials Engineering, Science and Technology Center, Federal University of Campina Grande, Av. Aprígio Veloso – 882, Bodocongó 58429 - 900, Campina Grande, PB, Brazil

Received 3 May 2020; accepted 2 September 2020

Available online 10 September 2020

KEYWORDS

Transesterification and esterification simultaneously;
Ferrite;
Heterogenous catalysis;
Reuse

Abstract A magnetic catalyst with composition ZnO-Ni_{0.5}Zn_{0.5}Fe₂O₄-Fe₂O₃ was synthesized by a combustion reaction on a pilot-scale and applied in the conversion of residual oil into biodiesel by simultaneous transesterification and esterification reactions (TES). For that, statistical analysis of the factors that influence the process (catalyst concentration, alcoholic route, and temperature) was evaluated by 2³ factorial experimental design. The ZnO-Ni_{0.5}Zn_{0.5}Fe₂O₄-Fe₂O₃ magnetic catalyst was characterized in terms of the structure, morphology, magnetic, TPD-NH₃ acidity analysis and catalytic properties. The results indicate the formation of a catalyst with a surface area of 52.9 m²g⁻¹, and density of the sample was 4.8 g/cm³ which is consisted of a mixture of the phases containing 55.87% Fe₂O₃, 36.96% Ni_{0.5}Zn_{0.5}Fe₂O₄, and 7.16% ZnO. The magnetic characterization indicated that the synthesized catalyst is ferromagnetic with magnetization 6.12 emu/g and coercive field of 5.3 G. In the TES reactions, the residual oil was active showing conversion to 96.16% ethyl esters and with a long useful life maintaining sustained activity after two consecutive reuse cycles with the conversion of 95.27%, 93.07% and 76.93%, respectively. The experimental design was significant and presented a 95% reliability level. The statistical analysis identified (+1) and (-1) as higher and lower level variables, respectively. The amount of catalyst used was equal to 5%, at

* Corresponding author.

E-mail address: adrianolimadasilva@hotmail.com (A.L. da Silva).

Peer review under responsibility of King Saud University.



200 °C in methyl alcohol (alcoholic route). In summary, a new catalyst composed of a mixture of magnetically active phases was developed and successfully applied in biodiesel's synthesis from residual oil. Undoubtedly these results have a positive and significant impact on the environment and to society as a whole.

© 2020 Published by Elsevier B.V. on behalf of King Saud University. This is an open access article under the CC BY-NC-ND license (<http://creativecommons.org/licenses/by-nc-nd/4.0/>).

1. Introduction

In recent years, researches on renewable and sustainable fuels have been highly prioritized around the world to create alternatives to fossil fuels. In this way, different types of biofuels have gained evidence due to their biodegradable, non-toxic, and physical–chemical properties, which allow the total or partial replacement of diesel (Li et al., 2014). Biofuels also are interesting under economic viewpoint since they can be synthesized from vegetable oils, animal fats, and raw materials rich in free fatty acids, such as residual oils (Lam et al., 2010).

The improper disposal of the residual oils can cause environmental problems since each liter of oil poured into the drain can pollute about 20 thousand liters of water (Georgogianni et al., 2009; Al-Hamamre and Yamin, 2014; Baskar et al., 2018). Indeed, it is possible to find in the literature several works (Widayat et al., 2019; Dai et al., 2017; Corro et al., 2016; Gan et al., 2010; Ashok et al., 2019) which the cook oils are used to synthesize biodiesel, and it is undoubtedly an eco-friendly and sustainable strategy for the next generations (Aghbashlo and Demirbas, 2016).

Biodiesel is synthesized via transesterification or esterification chemical reactions. In some cases, depending on the origin of the raw material (such as the presence of triglycerides and free fatty acids), the reaction kinetics can be directed by simultaneous transesterification and esterification. On an industrial scale, biodiesel can be produced by both homogeneous and heterogeneous catalysis. Homogeneous catalysis has several disadvantages, such as the formation of soaps and their by-products, corrosion of the reactors, in addition to requiring several purification steps during the production process (Lee et al., 2014; Avhad and Marchetti, 2015; Mardhiah et al., 2017). On the other hand, the synthesis of biodiesel via heterogeneously catalyzed reactions has been the subject of promising studies being a viable solution to replace homogeneous catalysis, since it is possible to significantly reduce the number of purification steps and the possibility of separating and reusing the catalyst (Correia et al., 2014; Rashtizadeh et al., 2014; Paiva et al., 2015; Kim et al., 2016).

In the heterogeneous catalysis, several types of catalysts stand out; however, ceramic compounds in the form of oxides (Baskar et al., 2018; Xie and Zhao, 2014; Gurunathan and Ravi, 2015; Sun et al., 2015; Sulaiman et al., 2019), have been extensively investigated in recent years for their high catalytic activity, excellent thermal and chemical stability, high corrosion resistance and environmentally optimized properties (Pradhan and Parida, 2012), and can be recovered and reused without significant loss efficiency in synthesis (Dantas et al., 2013).

Several chemical synthesis techniques can be used to obtain ceramic oxide catalysts, among them stand out the sol–gel route (Kesavamoorthi and Raja, 2016), co-precipitation

(Zaharieva et al., 2015), Pechini method (Gerasimov et al., 2015) and combustion reaction (Dantas et al., 2020). The combustion reaction, which is the chemical synthesis techniques used in this work, has stood out for being a simple, effective, economical method (it uses low-cost reagents, less reaction time), it allows control of stoichiometry and morphology, besides promoting the obtaining of high crystallinity ceramic powders (Costa and Kiminami, 2012). Due to its various advantages, numerous studies have reported the use of the combustion reaction in the production of materials applied in several areas, such as photocatalysis (Das et al., 2019; Hermosilla et al., 2020), electronic materials (Vieira et al., 2014; Shanmugavani et al., 2015; Tholkappiyar et al., 2015; Diniz et al., 2017), heterogeneous catalysis (Manikandan et al., 2014; Alaei et al., 2018; Dantas et al., 2020; Kombaiah et al., 2019; Mapossa et al., 2020), and biomaterials (Araújo et al., 2018; Khot et al., 2013; Kombaiah et al., 2018; Leal et al., 2018).

Among the oxides already reported in the literature with catalytic potential, the hematite (α -Fe₂O₃) with binary structure type A_nX_p is widely used in several catalysis reactions because it is stable in ambient conditions and easy to process by different methods (Aghbashlo and Demirbas, 2016; Gurunathan and Ravi, 2015; Tholkappiyar et al., 2015; Kombaiah et al., 2019; Widayat et al., 2019). Widayat et al. (2019) used hematite (α -Fe₂O₃) synthesized by chemical co-precipitation in residual oil esterification/transesterification reactions and obtained 87.88% conversions in methyl esters. Studies conducted by Shi et al. (2017) showed the efficiency of hematite (Fe₂O₃) also as the support of oxides (CaO) in the production of biodiesel, in transesterification reactions of soybean oil and methanol, showing conversion to esters of 98.80%.

Iron-based catalysts, such as ternary oxides of the type (AB₂X₄), have also attracted attention from the scientific community due to their properties and new technological applications, especially when the particle size approaches the nanoscale, which allows the control of properties such as magnetic characteristic and anisotropy (Dantas et al., 2020, Mapossa et al., 2020; Dai et al., 2017). In heterogeneous catalysis (Dantas et al., 2013, Dantas et al., 2017), the Ni_{0.5}Zn_{0.5}Fe₂O₄ and Ni_{0.7}Zn_{0.3}Fe₂O₄ ferrites synthesized by combustion reaction and tested the catalytic behavior in transesterification and esterification using methyl and ethyl routes, obtaining conversions in esters above 94%.

Another heterogeneous catalyst that has a consolidated catalytic activity in the literature is zinc oxide (ZnO). According to Lamba et al. (2019), which synthesized the ZnO by combustion reaction and tested catalytically against methanol and madhuca oil, obtaining about 80% in conversion into esters. Baskar et al. (2018) also revealed the efficiency of the ZnO phase as support for biodiesel production, presenting conversions of 95.20% in methyl esters.

In this work, the combustion reaction was used to synthesize a new magnetic catalyst with composition equal to $\text{ZnO-Ni}_{0.5}\text{Zn}_{0.5}\text{Fe}_2\text{O}_4\text{-Fe}_2\text{O}_3$. The material was synthesized in a pilot-scale (Costa and Kiminami, 2012) and characterized in terms of its structure, morphology, magnetic and catalytic properties. Also, its catalytic capacity was investigated on the synthesis (TES reaction) of biodiesel from residual oil.

2. Materials and methods

2.1. Raw materials

In this research, the $\text{ZnO-Ni}_{0.5}\text{Zn}_{0.5}\text{Fe}_2\text{O}_4\text{-Fe}_2\text{O}_3$ magnetic catalyst was synthesized via a combustion reaction from the following chemical reagents, nickel nitrate hexahydrate ($\text{Ni}(\text{NO}_3)_2 \cdot 6\text{H}_2\text{O}$), hexahydrate zinc nitrate ($\text{Zn}(\text{NO}_3)_2 \cdot 6\text{H}_2\text{O}$), iron (III) nitrate nonahydrate ($\text{Fe}(\text{NO}_3)_3 \cdot 9\text{H}_2\text{O}$) and urea. All chemical reagents used were purchased on the Dinâmica (Brazil) with purities between 98 and 99%. The performance of the catalyst was evaluated on the conversion of residual oil into biodiesel via simultaneous transesterification and esterification reactions (TES). The residual oil used was collected in pastry shops in the city of Campina Grande, located in Paraíba state - Brazil. The physicochemical parameters of the residual oil were accomplished in agreement with AOCS Cd 3d-63 standard, and the result showed a value of 14.8 ± 0.005 mg of KOH/g of sample, methyl alcohol (CH_3OH)-purity 99.8% (Dynamic) and ethyl alcohol ($\text{CH}_3\text{CH}_2\text{OH}$) - purity 99.5% (Dynamic).

2.2. Catalyst synthesis

The combustion reactions were accomplished in a pilot plant, which was built in the agreement of the patent BR 10 2012 002181-3 (Costa and Kiminami, 2012), see Fig. 1. The pilot-plant is constituted of the stainless-steel container, which is connected to a conical reactor with a capacity of 200 g/batch. The system reaches a maximum temperature equal to 350°C after 60 min.

Before the synthesis of the $\text{ZnO-Ni}_{0.5}\text{Zn}_{0.5}\text{Fe}_2\text{O}_4\text{-Fe}_2\text{O}_3$ magnetic catalyst, the initial composition of the precursor solution was calculated based on the total valence of oxidizing

agents and reducing reagents using the propellants and explosives chemistry concepts (Jain et al., 1981). The auto-ignition (combustion) of a stoichiometric mixture of metallic nitrates and urea allocated in a stainless-steel container in a conical reactor with a production capacity of 200 g/batch (see Fig. 1). The temperature of the combustion reaction was measured every 5 s with the aid of an infrared pyrometer (Raytek, model RAYR31 $\pm 2^\circ\text{C}$).

2.3. Catalytic test

The performance of the $\text{ZnO-Ni}_{0.5}\text{Zn}_{0.5}\text{Fe}_2\text{O}_4\text{-Fe}_2\text{O}_3$ magnetic catalyst was evaluated in the synthesis of biodiesel from residual oil via TES reaction. Before biodiesel synthesis, the residual oil was filtered (filter paper $\text{C}15,00' \pm 0,15$ cm) to remove the suspended particulate matter. The catalytic tests were conducted in duplicates and a pressurized stainless-steel reactor equipped with a pressure gauge, a thermocouple inlet duct, a borosilicate glass (80 mL). The conditions of the experiment were 30 g oil mass, time 1 h, and alcohol/oil ratio (15:1), see Table 1. The heating and agitation of the system were carried out with the aid of a plate model IKA C-MAG HS 7, external electrical resistance, and a magnetic bar of approximately 2.5 cm. After the reactions, the products of the catalytic tests were centrifuged to separate the catalyst, purified, and dried in an oven at 110°C for 20 min with manual stirring at 5-minute intervals.

2.4. Statistical analysis

For the analysis and optimization of the biodiesel synthesis from residual oil, a 2^3 factorial experimental design was drawn up in which it was analyzed the response surface and Pareto graph, evaluated using the Statistic 7.0 program. Table 1 describes the input levels and variables for the proposed planning.

The temperature, catalyst concentration, and alcoholic route were the factors considered in the 2^3 factorial experimental design. The three levels for the selected factors were determined from preliminary experiments and literature published elsewhere (Dantas et al., 2020) (Table 1). The conversion of residual oil into biodiesel was performed as the answer to

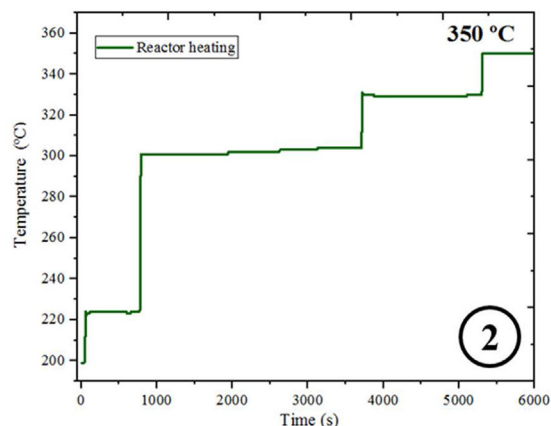


Fig. 1 Shows (1) pilot plant in which the combustion reaction was performed (patent number: BR 10 2012 002181-3) e (2) reactor heating curve.

Table 1 Input variables and levels proposed for 2³ factorial experiments.

Variables	Levels	
	-1	+1
(1) Catalyst concentration (%)	3	5
(2) Temperature (°C)	180	200
(3) Alcoholic route	MET	ET

*Fixed conditions: 30 g oil mass, time 1 h, and alcohol/oil ratio (15:1).

determine the optimized parameters. The effect of the independent factors on dependent factors was analyzed according to Eq. (1):

$$Y = a_0 + a_1X_1 + a_2X_2 + a_3X_3 + a_{12}X_1X_2 + a_{13}X_1X_3 + a_{23}X_2X_3 + e, \quad (1)$$

where Y is the answer (biodiesel conversion, %), a_0 is the compensated term; a_1 , a_2 e a_3 are linear coefficients; a_{12} , a_{13} , and a_{23} are the interaction coefficients; and e is the error. X_1 , X_2 e X_3 are input variables: temperature, the quantity of catalyst, and alcoholic route, respectively.

2.5. Catalyst reuse

The reuse tests were accomplished under the best reaction conditions established by the experiments and experimental planning. Before each reuse step, the ZnO-Ni_{0.5}Zn_{0.5}Fe₂O₄-Fe₂O₃ magnetic catalyst was removed from the synthesis products and clean with water 70 °C and hexane 99% (C₆H₁₄). After biodiesel synthesis, the catalyst was removed from the reaction medium using the following experimental procedure: application of an external magnetic field (magnet), washing with hot distilled water (~60 °C), washing the hexane solvent, centrifugation for 15 min, and oven drying at 110 °C for 24 h. This experimental procedure was adapted from the work published by Dantas et al. (2020). Finally, the reuse tests were performed under the best reaction conditions established by the experiments and experimental planning with the tested catalyst.

2.6. Characterizations

The ZnO-Ni_{0.5}Zn_{0.5}Fe₂O₄-Fe₂O₃ magnetic catalyst synthesized was characterized by X-ray diffraction (XRD) using a BRUKER X-ray diffractometer (model D2 PHASER, Cu-K α radiation), operating with 30 kV and 10 mA. The angular step and counting time used were 0.016° and 44 min, respectively. The crystallite size was calculated with the aid of the Scherrer equation (Klug and Alexander, 1974), and from the peak of the most intense basal reflection, spinel d(311). The identification of the main crystalline phases was performed with the DiffracPlus Suite Eva software and Joint Committee on Powder Diffraction Standards (JCPDS). The quantification of each main crystalline phase was carryout by the Rietveld refinement (Rietveld, 1967; Moulton, 2019) with the aid of Diffrac. Topas software. The residual error of the Rietveld refinement was calculated from Eq. (2), which $W_i = 1/I_{obs}$ and I_{obs} e I_{calc} are the observed and calculated intensities for each step, respectively.

$$Sy = \sum_i W_i (I_{Obs} - I_{Calc})^2 \quad (2)$$

The surface of the catalyst was characterized using the nitrogen gas adsorption and desorption technique. All experiments were carried out in a Quantachrome model NOVA 3200 equipment. The surface area and pore diameter were calculated using the Brunauer, Emmett, and Teller (BET) and by Brunauer, Joyner, and Halenda (BJH) methods, respectively.

The morphological aspects of the catalyst sample were acquired by scanning electron microscopy (SEM), brand TESCAN, model Vega3. The Laser diffraction technique was used to measure the particle size distribution using a nanoparticle analyzer SZ-100 series (HORIBA Scientific).

Hysteresis plots were measured at room temperature using a vibrating sample magnetometer (VSM, Lake Shore model 7404), with a maximum applied magnetic field of 13,700 G. Saturation magnetization (M_s), remaining magnetization (M_r), and coercive field (H_c) were the properties obtained from this experiment.

The acidity of the catalyst was determined through desorption analysis at the programmed ammonia temperature (TPD-NH₃) in the SAMP3 multipurpose analysis system. Approximately 100 mg of sample was pretreated at 400 °C under helium atmosphere (30 mL.min⁻¹). Then, the temperature was reduced to 100 °C, and the sample was subjected to ammonia current, for chemical adsorption, for 45 min. In the final step of the adsorption process, NH₃ molecules were removed at 100 °C for 1 h and helium flow rate 30 mL.min⁻¹. The thermograms were obtained on heating (from 100 °C to 800 °C), at 10 °C.min⁻¹, and under a helium flow rate (30 mL.min⁻¹).

Thermogravimetric analysis (TG/DTG) was performed using Perkin Elmer STA 6000 TG-DTA equipment in N₂ atmosphere with the flow of 20 mL.min⁻¹ and heating rate of 10 °C.min⁻¹, using 10 mg of sample in an alumina crucible, and a temperature range from 30 to 850 °C;

The percentages of methyl or ethyl esters were determined via gas chromatography, using a chromatograph (VARIAN 450c) instrument with a flame ionization detector and a capillary column as the stationary phase (Varian Ultimetal "Select Biodiesel Glycerides RG"; dimensions: 15 m × 0.32 mm × 0.45 mm). The initial injection temperature was 100 °C, the oven temperature was 180 °C, and the detector operated at a temperature of 380 °C.

The acidity index (official AOCS method, Cd 3d-63) was used to characterize both the residual oil and the products resulting from the catalytic tests. It was possible to quantify the mass yield of synthesized biodiesel, considering the initial mass of the residual oil in the TES reaction, assuming that the complete reaction of a specified amount (x) of residual oil leads to the achievement of 100% yield mass (X) of biodiesel. Therefore, the percentages of mass yields were defined and calculated as the values that express the masses of the final products of the reactions after the purification processes.

3. Results and discussion

3.1. Influence of reaction time and temperature on catalyst synthesis

Fig. 2 shows the combustion reaction behavior measured during the synthesis of the ZnO-Ni_{0.5}Zn_{0.5}Fe₂O₄-Fe₂O₃ magnetic

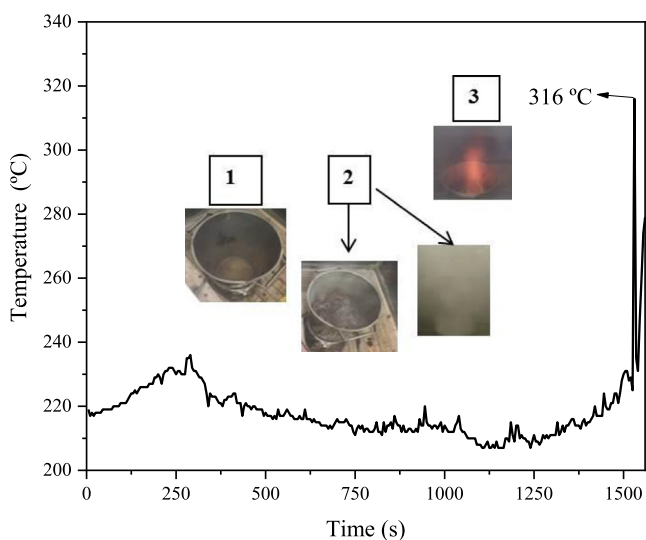


Fig. 2 Shows the combustion reaction behavior measured during the synthesis of the $\text{ZnO-Ni}_{0.5}\text{Zn}_{0.5}\text{Fe}_2\text{O}_4\text{-Fe}_2\text{O}_3$ magnetic catalyst.

catalyst. In summary, it was possible to identify three stages, where stage 1 was characterized by an oscillation in temperature that favored the evaporation of moisture followed by liquefaction of the reagents. In stage 2, the formation of the “mushroom” was observed (due to an increase in viscosity), followed by an excessive gas release. The ignition of the reagents combustion occurred in the final part of stage 2 (~1500 s). Stage 3 was instantaneous (~10 s) and reached a maximum temperature of 316 °C. In this last stage, there was the formation of an orange flame with a continuous and intense gas release. Still in step 3, it was possible to see a reaction explosion with flaking of the reaction product. The yield of the synthesis of the $\text{ZnO-Ni}_{0.5}\text{Zn}_{0.5}\text{Fe}_2\text{O}_4\text{-Fe}_2\text{O}_3$ magnetic catalyst was 82.93%, more precisely 165.8 g of catalyst per batch.

As the maximum temperature reached during the synthesis was relatively low (< 500 °C), the materials synthesized have a high surface area, and a very pronounced nanometric characteristic, therefore, is suitable for its use as catalysts. This constitutes ease and versatility of the combustion reaction technique because, due to the control of the synthesis temperature, it becomes possible the morphological and structural control of the material, which is required for a given application (Dantas et al., 2017).

3.2. X-ray diffraction (XRD)

Fig. 3 shows X-ray diffraction obtained from the $\text{ZnO-Ni}_{0.5}\text{Zn}_{0.5}\text{Fe}_2\text{O}_4\text{-Fe}_2\text{O}_3$ magnetic catalyst synthesized via a combustion reaction. The following crystalline phases were identified, inverse spinel of Ni-Zn ferrite (JCPDS 52-0278), hematite (JCPDS 89-0599), and zinc oxide (JCPDS 36-1451). The total crystallinity of the synthesized material was estimated at 43%, and the average crystallite size (calculated by Scherrer equation (Klug and Alexander, 1974; Avila et al., 2019) was equal to 25 nm. The estimated low crystallinity presented probably is related to the low-temperature of synthesis of the catalyst via combustion reaction (316 °C, see Fig. 2).

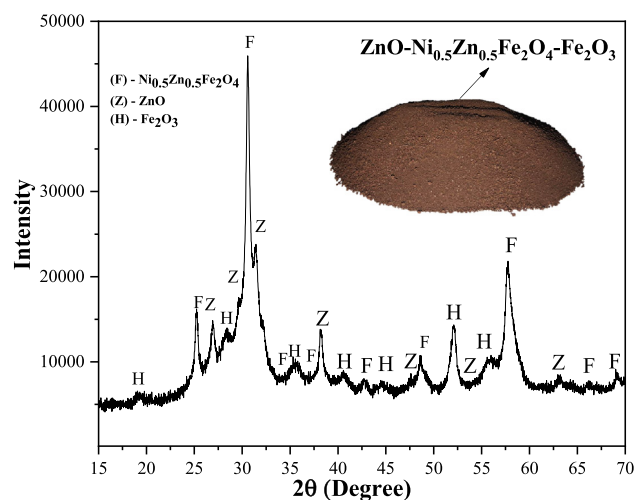


Fig. 3 X-ray diffractogram obtained from $\text{ZnO-Ni}_{0.5}\text{Zn}_{0.5}\text{Fe}_2\text{O}_4\text{-Fe}_2\text{O}_3$ magnetic catalyst.

This result is in agreement with other works that synthesized materials via combustion reaction and with a chemical composition similar to the one studied in this work (Dantas et al., 2020; Mapossa et al., 2020).

Fig. 4 shows the Rietveld refinement accomplished on the X-ray diffractogram obtained from a $\text{ZnO-Ni}_{0.5}\text{Zn}_{0.5}\text{Fe}_2\text{O}_4\text{-Fe}_2\text{O}_3$ magnetic catalyst. From this analysis, it was possible to see that the hematite was the major crystalline phase (55.87%); the inverse spinel of Ni-Zn ferrite was the second most abundant crystalline phase (36.96%), and zinc oxide was the crystalline phase with the lowest percentage (7.16%). **Table 2** summarizes the crystalline system, percentage of the crystalline phases, and the space groups calculated from the Rietveld refinement. In general, it is observed that the calculated parameters were very close to the theoretical values, and the values of the GOF, R_{wp} , and R_{exp} were 2.87, 0.99, and 0.35, respectively. Similar results were related by Mapossa et al. (2020).

3.3. Textural analysis by nitrogen adsorption (BET)

Fig. 5 shows the N_2 adsorption/desorption isotherms measured from the $\text{ZnO-Ni}_{0.5}\text{Zn}_{0.5}\text{Fe}_2\text{O}_4\text{-Fe}_2\text{O}_3$ magnetic catalyst. The isotherm obtained is of type III; which is an indication that the adsorption process is characteristic of non-porous or macroporous materials (Alothman, 2012). Also, the isotherms showed an inflection at a relative pressure (P/P_0) of approximately 0.2 cm^3/g , which is also indicative of the presence of micropores (Alothman, 2012).

In agreement with IUPAC, solids containing pores diameter greater than 50 nm are called macroporous, between 2 and 50 nm are mesoporous, and those with pores smaller than 2 nm are called of microporous. The measured pore diameter from the $\text{ZnO-Ni}_{0.5}\text{Zn}_{0.5}\text{Fe}_2\text{O}_4\text{-Fe}_2\text{O}_3$ magnetic catalyst was equal to 3.33 nm. Thus, the pore diameter and the isotherm profile corroborate with the indication that the synthesized catalyst has a mixed surface, that is, non-porous regions and other regions that have mesoporous or microporous.

The specific surface area values (S_{BET}) measured from the $\text{ZnO-Ni}_{0.5}\text{Zn}_{0.5}\text{Fe}_2\text{O}_4\text{-Fe}_2\text{O}_3$ catalyst was $52.9 \text{ m}^2\text{g}^{-1}$. This

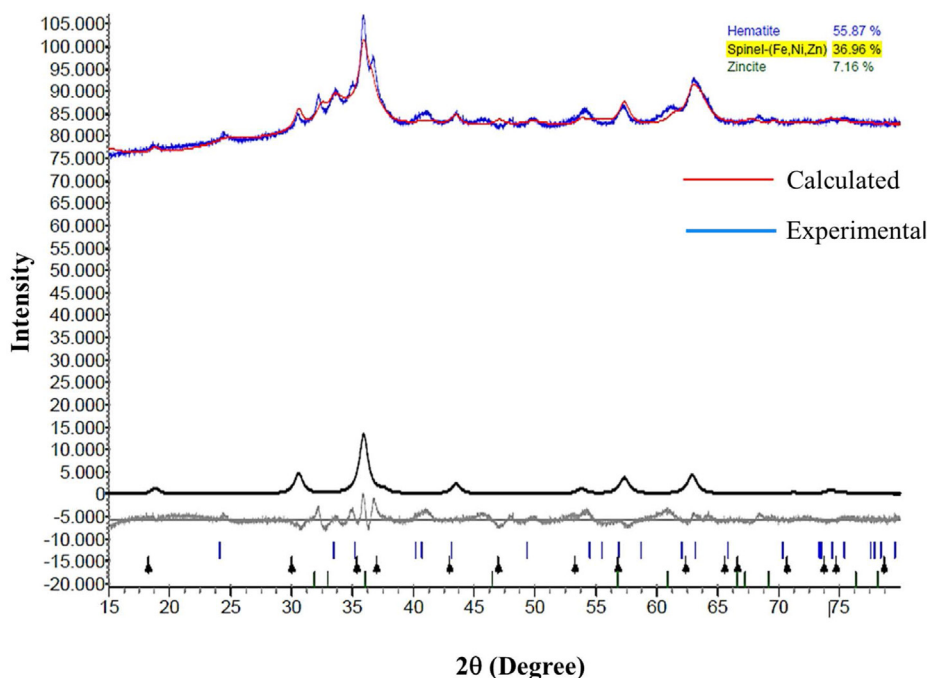


Fig. 4 Rietveld refinement accomplished from the X-ray diffractogram of the $\text{ZnO-Ni}_{0.5}\text{Zn}_{0.5}\text{Fe}_2\text{O}_4\text{-Fe}_2\text{O}_3$ magnetic catalyst.

Table 2 Shows the space group, crystalline, and percentage of the phases calculate from Rietveld analysis.

Lattice parameters (Å)	crystalline system	crystalline phases (%)	space groups
$a = 5.09$ e $c = 13.45$ Reference*: $a = 5.02$ e $c = 13.73$	Fe_2O_3 (Rhombohedral)	55.87	$R\text{-}3cH$
$a = b = c = 8.41$ Reference*: $a = b = c = 8.38$	Ferrite (Ni-Zn) (Cubic)	36.96	$Fd\text{-}3mZ$
$a = 3.23$ e $c = 5.42$ Reference*: $a = 3.24$ e $c = 5.20$	ZnO (Hexagonal)	7.16	$P63mc$

* Reference based on crystallographic cards: Fe_2O_3 (JCPDS 89-0599), ferrite (Ni-Zn-Fe (JCPDS 52-0278), and ZnO (JCPDS 36-1451).

value is considered relatively high and is a consequence of the method used to synthesize the catalyst (combustion reaction at temperatures below 500 °C). The fact of the $\text{ZnO-Ni}_{0.5}\text{Zn}_{0.5}\text{Fe}_2\text{O}_4\text{-Fe}_2\text{O}_3$ has a relatively high specific surface area and nanometric characteristics make it an excellent candidate to be used as a catalyst. Some studies report that the synthesis temperature is a significant factor in obtaining materials with high surface area and nanometric characteristics. Materials synthesized at high temperatures (> 1000 °C) have surface changes that are more pronounced, and in some cases, these modifications considerably reduce the surface area and active sites of catalysts, which negatively affect their catalytic activity (Tang et al., 2012).

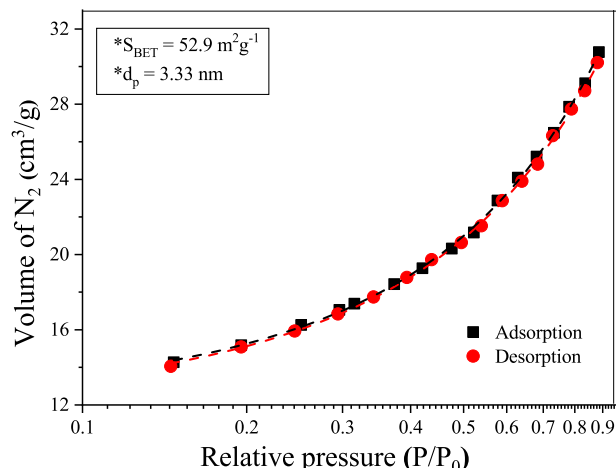


Fig. 5 N_2 adsorption/desorption isotherms of the $\text{ZnO-Ni}_{0.5}\text{Zn}_{0.5}\text{Fe}_2\text{O}_4\text{-Fe}_2\text{O}_3$ magnetic catalyst, in which S_{BET} and d_p correspond to specific surface area and pores diameter, respectively.

3.4. Scanning electron microscopy (SEM) and particle size distribution

Fig. 6a–b shows SEM images obtained from the $\text{ZnO-Ni}_{0.5}\text{Zn}_{0.5}\text{Fe}_2\text{O}_4\text{-Fe}_2\text{O}_3$ magnetic catalyst. It is possible to observe several clusters of different sizes (Fig. 6a). This characteristic is more evident in Fig. 6b, where it was possible to detect agglomerates with high porosity and dimensions between 20 μm and 10 μm , respectively. These results are in line with the discussion as mentioned earlier about the specific surface area analysis when it is indicated that the catalyst obtained has disordered surface characteristics with non-

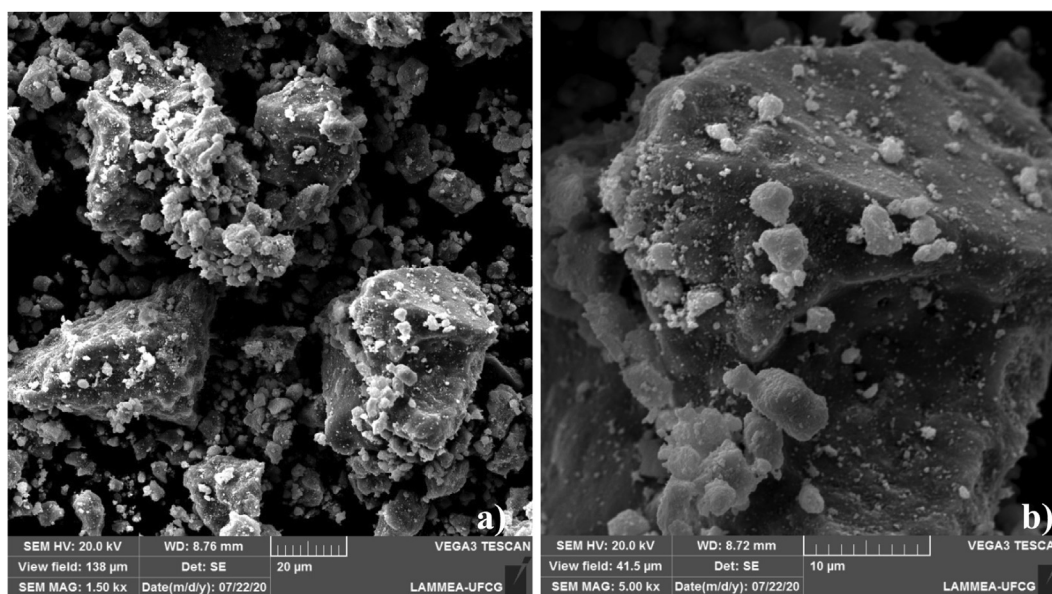


Fig. 6 a–b SEM images acquired from the surface of the ZnO-Ni_{0.5}Zn_{0.5}Fe₂O₄-Fe₂O₃ magnetic catalyst.

porous regions and other regions that have mesopores or micropores with different types of shapes and sizes. The high porosity is due to the release of large quantities of gas during the synthesis process by combustion reaction (see step 3 in Fig. 2). Still in Fig. 6a–b, both indicate a surface with a certain roughness, it is also possible to infer that the particles are weakly connected in an interparticular way. Similar results were observed by [Tatarchuk et al. \(2020\)](#) when studying the morphology of zinc spinel type ferrites.

Fig. 7 shows the cumulative curve of the distribution range of the agglomerates (“S” shape) and histogram of the frequency of the distribution of agglomerate populations with the same diameter (first derivative of the distribution curve) measured from the ZnO-Ni_{0.5}Zn_{0.5}Fe₂O₄-Fe₂O₃ magnetic catalyst. The distribution range of the particle diameter was between 20 nm and 100 nm, with an average diameter of 39.2 nm.

From the distribution of the clusters, it was possible to observe that all samples showed a symmetrical and monomodal distribution of clusters, indicating samples with most of the total number of their clusters, as well as a finer particle size between them (values < 100 nm). Such a result can be associated with the characteristics of particle size; smaller particle diameters necessarily imply a more remarkable ability to agglomerate by electrostatic forces.

3.5. Acidity of the catalysts via -NH₃-TPD

The structure, shape, and reactivity of the catalyst surface have a strong interaction with nature, the number and the intensity of the active sites available for the reaction. Thus, the reactivity of the catalyst surface is one of the inherent characteristics and its processing method. Therefore, to obtain a better precision of the surface reaction and to verify if this material is promising for catalysis, one must understand the acidity and alkalinity of the catalyst. ([Dantas et al., 2017](#)). In this way, the active acid sites of ZnO-Ni_{0.5}Zn_{0.5}Fe₂O₄-Fe₂O₃ were determined via TPD-NH₃ analysis, see Fig. 8.

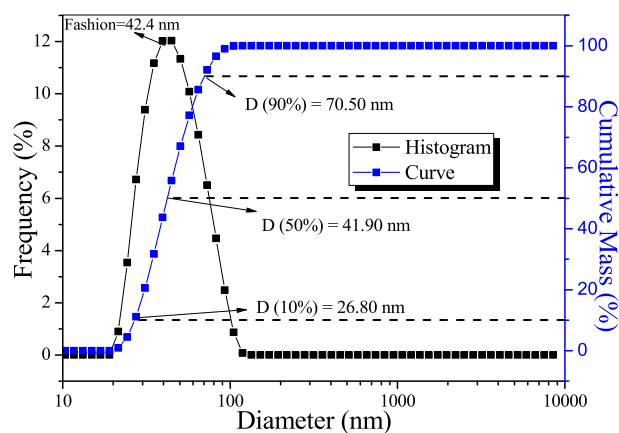


Fig. 7 Granulometric distribution of the ZnO-Ni_{0.5}Zn_{0.5}Fe₂O₄-Fe₂O₃ magnetic catalyst.

Still in Fig. 8, it is possible to identify three NH₃ desorption peaks. The first peak presented greater intensity, occurred at 208 °C, and is related to weak to moderate acidic sites. The second and third peaks occurred at 493 °C and 595 °C, respectively. These peaks are related to the strong acidic sites. The temperatures and intensity of the peaks observed in this work are in agreement with [Dantas et al. \(2017\)](#) and [Dantas et al. \(2020\)](#).

Table 3 lists the results obtained from the TPD analysis. The acidity of the ZnO-Ni_{0.5}Zn_{0.5}Fe₂O₄-Fe₂O₃ catalyst was calculated from the integration of the Gaussian curves observed in the TPD-NH₃ analysis. The result indicated the existence of two types of NH₃ desorption sites, which the first peak related to weak and moderate acid sites, represented by the temperature range between 100 and 350 °C, while the strong acidity sites are in the range temperature between 450 and 650 °C. Similar results were also reported by [Masiero et al. \(2009\)](#).

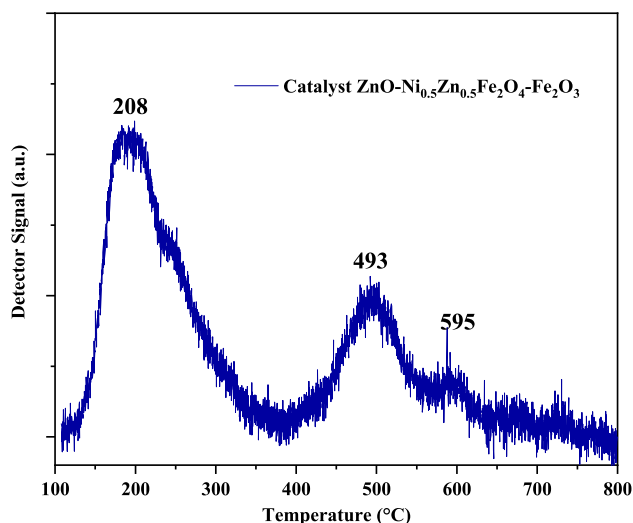


Fig. 8 TPD-NH₃ curve for the catalyst ZnO-Ni_{0.5}Zn_{0.5}Fe₂O₄-Fe₂O₃.

Therefore, from TPD-NH₃ analysis, the desorption events present in the samples showed concentrations corresponding to weak, moderate, strong acidic sites, and the calculated values were 169, 73, and 14 μmol/g of NH₃, respectively. The sample had a total acidity of 256 μmol/g of NH₃. From the highlighted results, it is possible to conclude that the ZnO-Ni_{0.5}Zn_{0.5}Fe₂O₄-Fe₂O₃ magnetic catalyst has a strong acid character. Also, the results shown in this work corroborate with studies published by Dantas et al. (2020) and Mapossa et al. (2020), which investigated acidic sites by means TPD-NH₃ analysis, and confirmed the presence of weak, moderate, and strong total acidic sites for spinel-type ferrites with composition chemistry, structure, and morphology similar to those synthesized in this work.

3.6. Magnetic measures

Fig. 9 shows the dependence of magnetization (*M*) as a function of the applied magnetic field (*H*) for the ZnO-Ni_{0.5}Zn_{0.5}Fe₂O₄-Fe₂O₃ magnetic catalyst. From the hysteresis curve, it is possible to conclude that the studied catalyst has characteristics of soft magnetic materials. The low values of remaining magnetization (*M_r* = 6.12 emu/g) and coercivity (*H_c* = 5.3 G) support this information, since the magnetic hysteresis cycle is shown is narrow. Also, the well-defined S shape of the hysteresis curve is indicative that the ZnO-Ni_{0.5}Zn_{0.5}Fe₂O₄-Fe₂O₃ magnetic catalyst has ferrimagnetic properties (Wang et al., 2012; Nihore et al., 2019).

Also, in Fig. 9, the low value of the remaining magnetization (*M_r*) observed can be explained in terms of the composi-

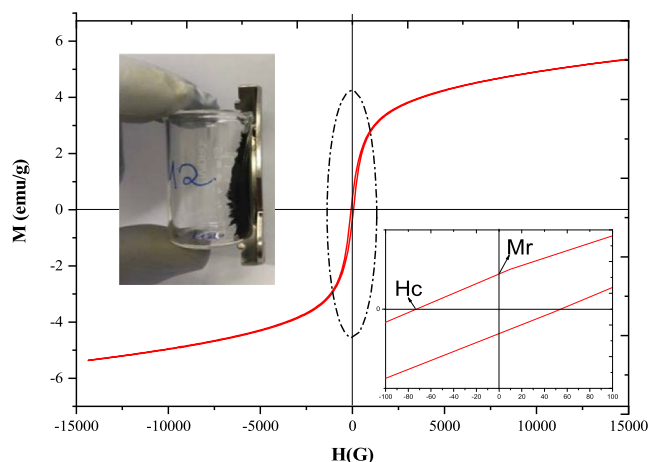


Fig. 9 Hysteresis curves (*M* × *H*) measured from the ZnO-Ni_{0.5}Zn_{0.5}Fe₂O₄-Fe₂O₃ catalyst.

tion of the ZnO-Ni_{0.5}Zn_{0.5}Fe₂O₄-Fe₂O₃ magnetic catalyst, since there is coexistence between crystalline ferromagnetic phases (55% Fe₂O₃), (36.96% Ni_{0.5}Zn_{0.5}Fe₂O₄) (Dantas et al., 2020; Shi et al., 2017), and diamagnetic phase (7.16% ZnO) (Franco et al., 2017). Similar results have been reported in the literature (Diniz et al., 2017) for the Ni-Zn system by microwave energy, where its magnetic characteristics are of a ferrimagnetic material (Hajalilou et al., 2015). Also obtained Ni-Zn ferrites synthesized by high-energy grinding and found that their magnetic hysteresis characteristics were presented in an “S” format with a unique coercive field. The results of this work corroborate those reported in the literature, emphasizing that the material is magnetic and its application in obtaining biodiesel because under the incidence of an external magnetic field, the catalyst will be easily removed from the reaction medium and thus reused.

The fact that the ZnO-Ni_{0.5}Zn_{0.5}Fe₂O₄-Fe₂O₃ catalyst has magnetic properties can help minimize the cost of biodiesel production since the catalyst can be easily removed from the reaction medium by applying an external magnetic field (magnet). Thus, magnetic separation is a relevant alternative to filtration and/or centrifugation since it contributes to reducing the loss of the catalyst and increases the reuse capacity, making the cost-benefit of the catalysts quite promising for industrial applications (Vieira et al., 2014).

3.7. Performance of the ZnO-Ni_{0.5}Zn_{0.5}Fe₂O₄-Fe₂O₃ magnetic catalytic

Fig. 10 shows the conversion of residual oil into esters and the mass yield obtained from the TES reaction through the ethyl

Table 3 Type of acidity present in catalyst magnetic ZnO-Ni_{0.5}Zn_{0.5}Fe₂O₄-Fe₂O₃.

Catalyst	Peak	Temperature (°C)	Acidity (μmol/g de NH ₃)	Type of Acidity
ZnO-Ni _{0.5} Zn _{0.5} Fe ₂ O ₄ -Fe ₂ O ₃	1	208	169	Weak/Moderate
	2	493	73	Strong
	3	595	14	Strong
Total acidity = 256 μmol/g de NH₃				

and methyl routes catalyzed by ZnO-Ni_{0.5}Zn_{0.5}Fe₂O₄-Fe₂O₃. All experiments were accomplished in agreement with the experimental planning indicated in Table 1. In general, it was possible to observe (Fig. 10) that the ZnO-Ni_{0.5}Zn_{0.5}Fe₂O₄-Fe₂O₃ catalyst was active and satisfactory conversions were obtained in esters of fatty acids, in 96.1% ethanolysis, and 92.5% methanolysis. The best catalytic activity was obtained for the ethyl route, which is beneficial for the process since the alcohol used is less polluting and comes from the culture of sugarcane (Shikida and Bacha, 1998). The efficiency of the ZnO-Ni_{0.5}Zn_{0.5}Fe₂O₄-Fe₂O₃ magnetic catalyst may be associated with the presence of acidic and basic sites (see the results obtained in Section 3.6), which gives the system great versatility, such as the possibility of conducting simultaneous esterification and transesterification reactions.

The experimental data shown in Fig. 10 also made it possible to observe that the profile of mass yield in biodiesel corroborates the profile of conversion into ethyl esters obtained from the tested reaction condition that showed the best catalytic activity, i.e., 30 g oil mass, time 1 h, and alcohol/oil ratio 15/1, 5% by weight of catalyst and 200 °C.

Besides, regard to the percentage of acidity index reduction (Fig. 10), it was possible to verify that in all reactions, there were still unreacted free fatty acids. However, this occurs with greater emphasis on milder conditions of the percentage of cat-

alyst and temperature. For example, using 3% catalyst and 180 °C, there was a reduction in the acidity of biodiesel by an average of only 44%, on the other hand, when elevated conditions reactions of the percentage of catalyst (5%) or temperature (200 °C), occurs a greater consumption of the fatty material available in the reaction, causing percentages of acidity reduction and conversions in higher esters, respectively, in the methyl route (88.4% and 92.5%) and the ethyl route (84.4% and 96.2%) using the so-called optimal conditions.

3.8. Statistical analysis

Oprime et al. (2017) emphasize in its research the importance of developing and using a formulation well resolved by process optimization methods through experimental planning, thus reporting the gain in time and amount of experiments as well as total process costs. In this context, in the present work, the statistical study was carried out, and Table 4 describes the planning matrix used to analyze the statistical data on biodiesel production from reaction TES, using the magnetic catalyst and residual oil through the routes methanolic and ethanolic.

Based on Table 4, it was possible to infer that the best catalytic condition for biodiesel's synthesis from residual oil was verified in experiment 7 since this favored a higher conversion

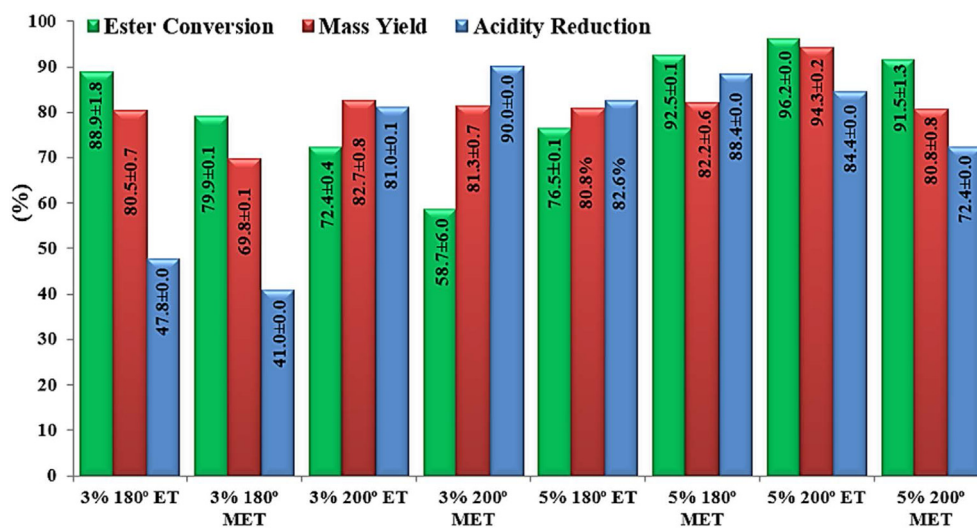


Fig. 10 Shows the percentage results of the effective mass yields, conversion of the residual oil into ethyl, and methyl esters obtained in the presence of the ZnO- ZnO-Ni_{0.5}Zn_{0.5}Fe₂O₄-Fe₂O₃ catalyst.

Table 4 Planning matrix obtained for the chosen random variables.

Run	Catalyst (%)	Temperature (°C)	Alcoholic route	Conversion 1	Conversion 2	Average Conversion
1	3	180	ET	87.0	90.8	88.9 ± 1.8
2	3	180	MET	79.7	80.1	79.9 ± 0.1
3	3	200	ET	72.8	71.9	72.4 ± 0.4
4	3	200	MET	64.7	52.6	58.7 ± 6.0
5	5	180	ET	76.3	76.6	76.5 ± 0.1
6	5	180	MET	92.6	92.3	92.5 ± 0.1
7	5	200	ET	95.7	96.5	96.2 ± 0.0
8	5	200	MET	90.1	92.8	91.5 ± 1.3

into esters (96.16 ± 0.08). Still, it was possible to verify that was obtained using ethyl alcohol, which is beneficial because besides being considered less toxic, it is produced directly from sugarcane. It is relevant to highlight that Brazil in the world ranking, is among the largest producers of sugarcane, trailing only Colombia, Australia, China, and the USA.

The responses of the statistical analysis carried out for the synthesis of biodiesel by TES from residual oil were evaluated using the Pareto graph, see Fig. 11.

Analyzing the Pareto Graph (Fig. 11), it is possible to observe that the statistical analysis indicates 95% reliability ($p < 0.05$) (Gan et al., 2010), showing as significant variables: quantity of catalyst (%), and temperature, as well as the effects of secondary interaction, the quantity of catalyst \times temperature (1by2), the quantity of catalyst \times alcoholic route (1by3), and the interaction between temperature \times alcoholic route (2by3). From this analysis, it was possible to conclude that the variable quantity of catalyst

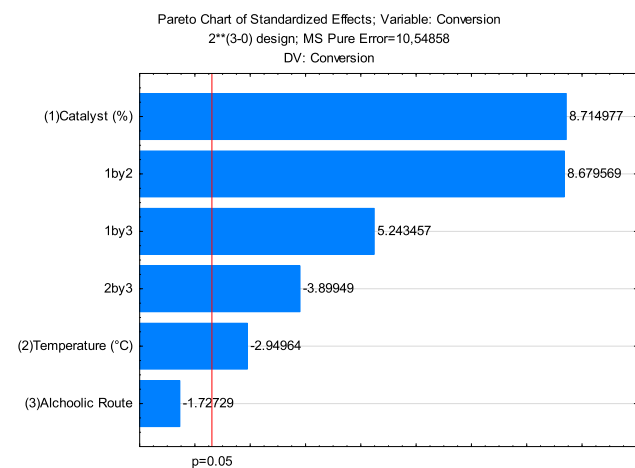


Fig. 11 Pareto graph resulting from 2^3 factorial planning for the conversion of biodiesel.

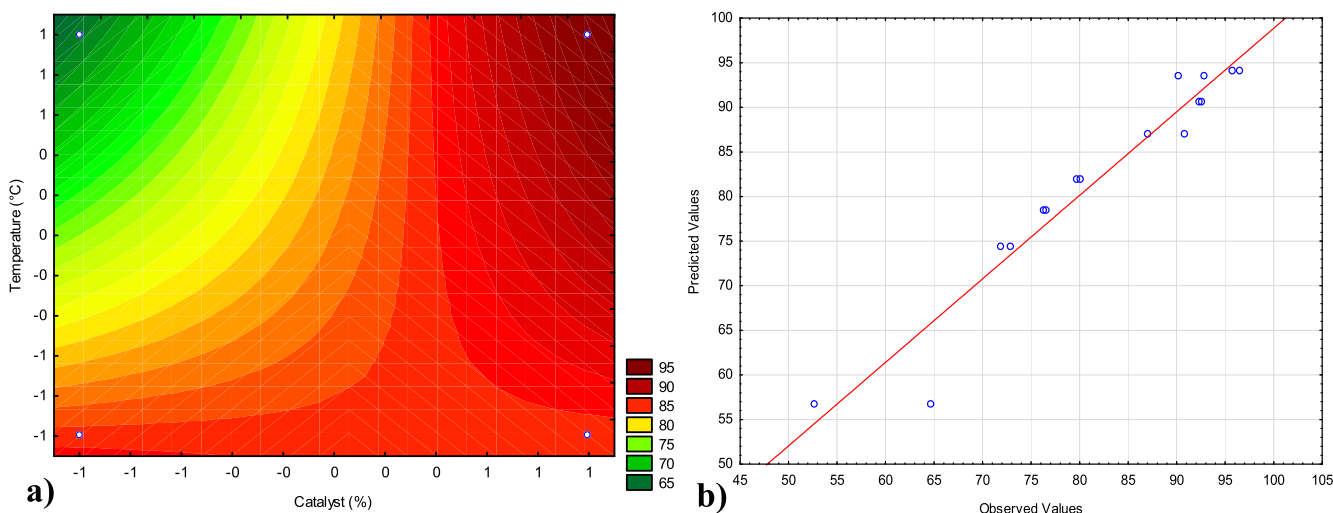


Fig. 12 (a) Curve level for biodiesel conversion with the interaction between temperature and quantity of catalyst; (b) Expected results versus experimental products of conversion to methyl/ethyl ester for the TES reaction. *The line corresponds to the zero error between the experimental and the predicted values.

(%) and the secondary interactions (1by2) and (1by3) had a positive influence. In contrast, the variable temperature and the secondary interaction (2by3) had an influence negative. These observations are confirmed through the data in Table 4 and Fig. 10, suggesting that a mass increase in the quantity of catalyst significantly increases the conversion of residual oil into biodiesel through TES reaction.

Fig. 12(a) illustrates the level curves obtained as a statistical response of the independent input variables: quantity of catalyst (%) and temperature. The reliability of the analysis was $p < 0.05$, see Fig. 11. Fig. 12(b) illustrates the results obtained from the linear regression model (Eq. (3)), which dependence between a dependent variable or response (the content of converted esters) and a series of values (predicted results) of the independent variables describes the experimental data versus the predicted ones.

The effect of secondary interaction between the percentage of catalyst and reaction temperature was better evaluated from the level curve (Fig. 12a). It was possible to observe that for high levels (+1) of temperature (200 °C), and quantity of catalyst (5%), the conversion of biodiesel was maximum (close to 100%), corroborating what was observed in the Pareto graph (Fig. 11). However, maintaining the upper level (+1) of the percentage of catalysts, at both temperatures studied, the conversion into esters remained at or above 85%. Therefore, it was possible to infer that the catalyst variable is the most significant and shows an excellent catalytic behavior of the $\text{ZnO-Ni}_{0.5}\text{Zn}_{0.5}\text{Fe}_2\text{O}_4\text{-Fe}_2\text{O}_3$ magnetic composite.

In the investigated region, the response surface is described satisfactorily by the linear mathematical model given by Eq. (3), which presented an R^2 of 94% and which defines the plane represented in perspective on the contour line (Fig. 12a), from according to the experimental planning carried out for the TES reaction of the residual oil, which best represents the data collected, analyzed and adjusting to the data in Table 4.

$$Y = 82.08375 + 7.07625 * x - 2.395 * y + 7.0475 * x * y + 4,2575 * 0. * x - ,16625 * 0. * y + 0. \quad (3)$$

The linear regression model (Fig. 12b) specifies the linear relationship between a dependent variable (or response) and a series of the predicted independent variables. This linear model governed by Eq. (3), represents a good description of the experimental data related to the content of the converted esters. It is possible to see in Fig. 12b that the results obtained experimentally are close to the values predicted by the model, considering that the modeling shows a correlation factor (R^2) equal to 0.94. This figure shows that the model represents a relatively good description of the experimental data related to the methyl/ethyl ester content at 1 h reaction time and the alcohol-oil ratio of 1/15. The modeling results showed that the most significant effects were the linear effects of the quantity of catalyst, temperature, and the combined effects between temperature, catalyst concentration, and alcoholic route. The other effects showed less significance.

The suitability of the linear model was also tested by analysis of variance (ANOVA) according to Table 5.

The ANOVA results (Table 5) for biodiesel production showed the F_{cal}/F_{tab} value of 6.54, which indicates that the model was statistically significant. Therefore, the regression model is given in Eq. (3) was a reasonable prediction of the experimental results, and the factors affected were real at a 95% confidence level, as already observed in Fig. 11. Based on all the statistical planning, we can conclude that the planning gives the optimized condition at a 95% confidence level. The maximum conversions in esters would be observed: upper level (+1) for the catalyst quantity variables (5%) and temperature (200 °C) and lower level (-1) for the alcoholic route variable (methyl route).

3.9. Reuse assessment

The recovery of magnetic particles for reuse in catalytic processes, in the most varied applications, has been highly reflected in the literature (Baskar et al., 2018; Dai et al., 2017; Guldhe et al., 2017). In the field of biodiesel production, some authors have already started to report excellent performances; for example, it is mentioned in (Ashok et al., 2019) with the use of nanoparticles of the ZnFe₂O₄Mn magnetic catalyst. Saxena et al. (2019), using magnetic Fe III nanocatalysts doped with ZnO, obtained high catalytic activity for the production of biodiesel, around $90 \pm 2\%$, and exhibited excellent transesterification capacity after its reuse. About the reuse of heterogeneous catalysts, this is one of the advantages high-

lighted in the literature and in this case, those catalysts with intrinsic magnetism are considered an advantageous resource, as they can promote different results in terms of recovery and reuse (Dantas et al., 2020; Farias et al., 2020).

In this context, the ZnO-Ni_{0.5}Zn_{0.5}Fe₂O₄-Fe₂O₃ magnetic catalyst was reused in the TES reaction using the optimized conditions: 30 g oil mass, time 1 h, and 15/1 alcohol/oil ratio, 5% by weight of catalyst and 200 °C. The conversion results obtained on reuse are illustrated in Fig. 13.

Based on Fig. 13, it is possible to see that after 2 reuses, a loss of about 19.23% in efficiency in the catalytic activity was found. However, it was found that the catalyst showed an average conversion of $90.29 \pm 0.44\%$. Therefore, the magnetic catalyst sample is economically viable for practical industrial applications.

To assess possible structural modification on the ZnO-Ni_{0.5}Zn_{0.5}Fe₂O₄-Fe₂O₃ catalyst during the TES reaction, thermogravimetry analyses were performed before the first catalytic test, and XRD analyses were accomplished before and after the catalytic tests.

As shown in Fig. 14(a), there was no significant structural change in the catalyst after evaluating its useful life, when comparing the two diffractograms before and after the TES reaction. Also, it was possible to observe that the structural parameters remained unchanged, i. e., crystallinity and crystal-

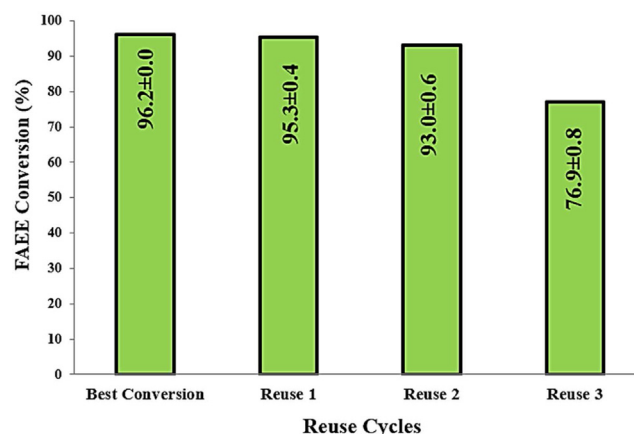


Fig. 13 Results of reuse tests obtained from the ZnO-Ni_{0.5}Zn_{0.5}Fe₂O₄-Fe₂O₃ magnetic catalyst in TES reactions.

Table 5 ANOVA to optimize the production of biodiesel from residual oil using a catalyst ZnO-Ni_{0.5}Zn_{0.5}Fe₂O₄-Fe₂O₃.

Variation Source	Quadratic Sum	Degree of Freedom	Quadratic Average	$F_{Calculated}$	F_{cal}/F_{tab}
Regression	2169.52	6	361.59	22.06	6.54
Waste	147.51	9	16.39	—	—
Lack of Adjustment	63.12	1	63.12	5.98	1.13
Pure Error	84.39	8	10.55	—	—
Total	2317.03	15			
F tabulated Regression	3.37	6			
F tabulated Lack of Adjustment	5.32	9			
% Mx. Explained	93.63				
% Mx. Explainable	96.36				
R^2	0.94				
Fit Quality	0.89				
S (standard regression error)	4.05				

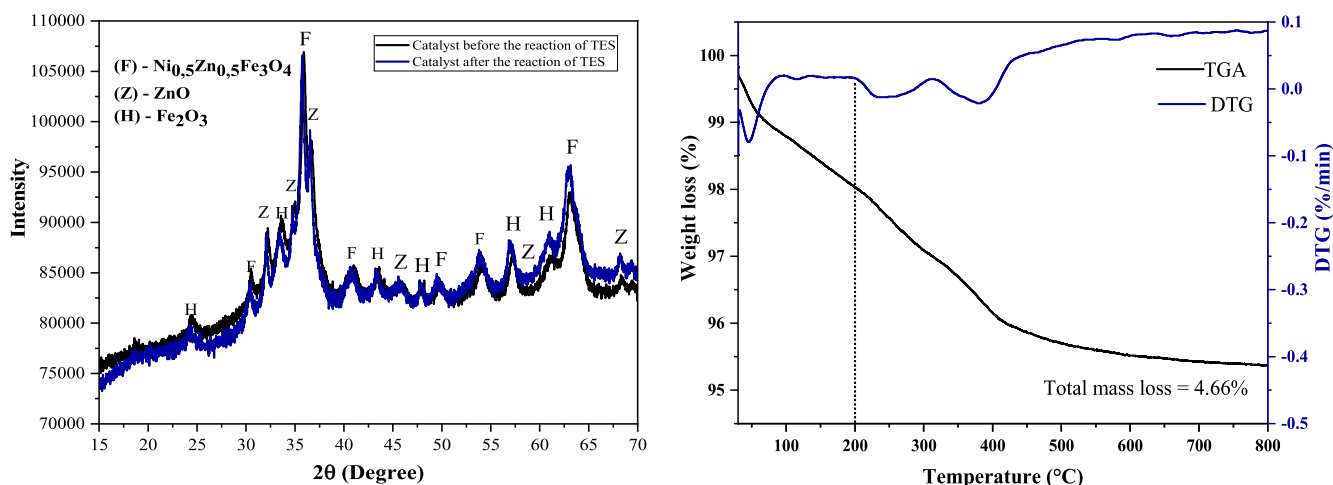


Fig. 14 (a) X-ray diffraction for the catalyst of $\text{ZnO-Ni}_{0.5}\text{Zn}_{0.5}\text{Fe}_2\text{O}_4\text{-Fe}_2\text{O}_3$ before and after the TES reaction, (b) Thermogravimetric analysis (TGA) of the catalyst of $\text{ZnO-Ni}_{0.5}\text{Zn}_{0.5}\text{Fe}_2\text{O}_4\text{-Fe}_2\text{O}_3$ before the TES reaction.

lite size showed a value of 41.2% (before 43%) and 26 nm (before 25 nm). This characteristic was confirmed with the aid of thermogravimetric analysis (Fig. 14(b)), where it was possible to observe that in the range up to 200 °C (maximum temperature used in TES reaction), it refers to the mass loss corresponding to humidity. According to Farias et al. (2020), subsequent mass loss events are attributed to decomposition processes and do not interfere with the TES reaction, since that the temperatures (180 and 200 °C) used in this work were lower. It is also possible to verify that the catalyst shows up to 800 °C, a total loss of mass of only 4.66%, where stabilization is verified. This statement is consolidated in the literature (Silva et al., 2019; Dantas et al., 2020; Farias et al., 2020) that indicates the thermal stability of spinel-type ferrites, starting at 800 °C. Based on the above, it is evident that there was no structural modification in the catalyst produced after the TES reactions, and the thermal stability of the same was also proven.

These data suggest that the decrease in catalytic capacity of the catalyst after the second cycle of reuse may be related to the residual presence of triglycerides, and/or unconverted fatty acids and/or impurities arising from the frying process in the residual oil that were possibly adsorbed on the surface of the catalyst, preventing the participation of the active sites available for the reaction. Therefore, it becomes clear the need to optimize the cleaning process of the residual starting oil and the catalyst after TES reaction, for greater efficiency in subsequent reactions.

4. Conclusion

The $\text{Fe}_2\text{O}_3\text{-Ni}_{0.5}\text{Zn}_{0.5}\text{Fe}_2\text{O}_4\text{-ZnO}$ magnetic catalyst was synthesized on a pilot-scale using combustion reactions. The pilot-scale production was safe, reproducible, and efficient. The catalyst synthesized is ferrimagnetic (6.12 emu/g), polyphasic ($\text{Fe}_2\text{O}_3\text{-Ni}_{0.5}\text{Zn}_{0.5}\text{Fe}_2\text{O}_4$ - ZnO), nanometric (24 nm), and with high surface area ($S_{\text{BET}} = 52.9 \text{ m}^2\text{g}^{-1}$). Before, the use of factorial design made it possible to evaluate the process in a multivariate manner, leading to the identification of variables that significantly influenced the response vari-

able (conversion of residual oil into esters). The factorial design allowed to identify the influence of the variables (percentage of catalyst, alcoholic route, and temperature) on the TES reaction, which, according to the statistical study, the quantity of catalyst and temperature followed by secondary interactions between all input variables (percentage of catalyst, temperature, and alcoholic route), were the ones that most affected the value of the response variable, with a significance level of 95%. The catalyst was effective in all conditions tested with conversions from 58% to 96%, with significantly promising results in the ethyl route. From the results obtained, it can be concluded that the studied catalyst can be successfully applied in the production of biodiesel, as the advantages have surpassed traditional methods since this polyphasic catalyst is a new product with innovative, magnetically active, and sustainable characteristics, and had a catalytically active useful life for two reuse cycles.

Acknowledgments

The authors thank CAPES/CNPq for their financial support.

References

- Aghbashlo, M., Demirbas, A., 2016. Biodiesel: hopes and dreads 379 379 *Biofuel Res. J.* 3. <https://doi.org/10.18331/BRJ2016.3.2.2>.
- Alaei, S., Haghghi, M., Toghiani, J., Rahmani, B.V., 2018. Magnetic and reusable $\text{MgO/MgFe}_2\text{O}_4$ nanocatalyst for biodiesel production from sunflower oil: influence of fuel ratio in combustion synthesis on catalytic properties and performance. *Ind. Crops Prod.* 117, 322–332. <https://doi.org/10.1016/j.indcrop.2018.03.015>.
- Al-Hamamre, Z., Yamin, J., 2014. Parametric study of the alkali catalyzed transesterification of waste frying oil for Biodiesel production. *Energy Convers. Manage.* 79, 246–254. <https://doi.org/10.1016/j.enconman.2013.12.027>.
- Al-Othman, Z., 2012. A review: fundamental aspects of silicate mesoporous materials. *Materials* 5, 2874–2902. <https://doi.org/10.3390/ma5122874>.
- Araújo, P.M.A.G., Araújo, N.G., Silva, M.R., Bicalho, S.M.C.M., Costa, A.C.F.M., 2018. Estudo do efeito da modificação de superfície de Fe_3O_4 e CoFe_2O_4 para aplicação como carreador

- de fármaco. *Cerâmica*. 64, 466–476. <https://doi.org/10.1590/0366-69132018643722379>.
- Ashok, A., Kennedy, L.J., Vijaya, J.J., 2019. Structural, optical and magnetic properties of Zn_{1-x}MnxFe₂O₄ (0 ≤ x ≤ 0.5) spinel nano particles for transesterification of used cooking oil. *J. Alloys Compounds* 780, 816–828. <https://doi.org/10.1016/j.jallcom.2018.11.390>.
- Avhad, M.R., Marchetti, J.M., 2015. A review on recent advancement in catalytic materials for biodiesel production. *Renew. Sustain. Energy Rev.* 50, 696–718. <https://doi.org/10.1016/j.rser.2015.05.038>.
- Avila, P.R.T., Silva, E.P., Rodrigues, A.M., Aristizabal, K., Pineda, F., Coelho, R.S., Garcia, J.L., Soldera, F., Walczak, M., Pinto, H. C., 2019. On manufacturing multilayer-like nanostructures using misorientation gradients in PVD films. *Sci. Rep.* 9, 15898. <https://doi.org/10.1038/s41598-019-52226-1>.
- Baskar, G., Selvakumari, I.A.E., Aiswarya, R., 2018. Biodiesel production from castor oil using heterogeneous Ni doped ZnO nanocatalyst. *Bioresour. Technol.* 250, 793–798. <https://doi.org/10.1016/j.biortech.2017.12.010>.
- Correia, L.M., Saboya, R.M.A., Sousa, C.N., Cecilia, J.A., Rodriguez-Castellón, E., Cavalcante, C.L., Vieira, R.S., 2014. Characterization of calcium oxide catalysts from natural sources and their application in the transesterification of sunflower oil. *Bioresour. Technol.* 151, 207–213. <https://doi.org/10.1016/j.biortech.2013.10.046>.
- Corro, G., Sánchez, N., Pal, U., Bañuelos, F., 2016. Biodiesel production from waste frying oil using waste animal bone and solar heat. *Waste Manage.* 47, 105–113. <https://doi.org/10.1016/j.wasman.2015.02.001>.
- Costa, A.C.F.M., Ruth Herta Goldschmidt Aliaga Kiminami, (2012). Dispositivo para a produção de nanocompósitos cerâmicos em larga escala por reação de combustão e processo contínuo de produção de nanocompósitos, *Revista de Propriedade Industrial-RPI*, BR 10 2012 002181-3.
- Dai, Y.M., Kao, I.H., Chen, C.-C., 2017. Evaluating the optimum operating parameters of biodiesel production process from soybean oil using the Li₂TiO₃ catalyst. *J. Taiwan Inst. Chem. Eng.* 70, 260–266. <https://doi.org/10.1016/j.jtice.2016.11.001>.
- Dantas, J., Leal, E., Cornejo, D.R., Kiminami, R.H.G.A., Costa, A.C.F.M., 2020. Biodiesel production evaluating the use and reuse of magnetic nanocatalysts Ni_{0.5}Zn_{0.5}Fe₂O₄ synthesized in pilot-scale. *Arabian J. Chem.* 13, 3026–3042. <https://doi.org/10.1016/j.arabjc.2018.08.012>.
- Dantas, J., Leal, E., Mapossa, A.B., Cornejo, D.R., Costa, A.C.F.M., 2017. Magnetic nanocatalysts of Ni_{0.5}Zn_{0.5}Fe₂O₄ doped with Cu and performance evaluation in transesterification reaction for biodiesel production. *Fuel*. 191, 463–471. <https://doi.org/10.1016/j.fuel.2016.11.107>.
- Dantas, J., Santos, J.R.D., Cunha, R.B.L., Kiminami, R.H.G.A., Costa, A.C.F.M., 2013. Use of Ni-Zn ferrites doped with Cu as catalyst in the transesterification of soybean oil to methyl esters. *Mater. Res.* 16, 625–627. <https://doi.org/10.1590/S1516-14392013005000031>.
- Das, K., Majhi, D., Bhoi, Y.P., Mishra, B.G., 2019. Combustion synthesis, characterization and photocatalytic application of CuS/Bi₄Ti₃O₁₂ p-n heterojunction materials towards efficient degradation of 2-methyl-4-chlorophenoxyacetic acid herbicide under visible light. *Chem. Eng. J.* 362, 588–599. <https://doi.org/10.1016/j.cej.2019.01.060>.
- Diniz, V.C.S., Silveira, J.E.R.J., Cornejo, D.R., Kiminami, R.H.G.A., Costa, A.C.F.M., 2017. Influence of Zn²⁺ content on morphological and magnetic properties of Mn_{1-x}Zn_xFe₂O₄ ferrites synthesized on a large scale by combustion reaction. *Cerâmica*. 63, 210–215. <https://doi.org/10.1590/0366-69132017633662111>.
- Farias, A.F., de Araújo, D.T., da Silva, A.L., Leal, E., Pacheco, J.G., Silva, M.R., Kiminami, R.H., Costa, A.C.D.M., 2020. Evaluation of the catalytic effect of ZnO as a secondary phase in the Ni_{0.5}Zn_{0.5}Fe₂O₄ system and of the stirring mechanism on biodiesel production reaction. *Arabian J. Chem.* 13, 5788–5799. <https://doi.org/10.1016/j.arabjc.2020.04.016>.
- Franco, A., Pessoni, H.V.S., Ribeiro, P.R.T., Machado, F.L.A., 2017. Magnetic properties of Co-doped ZnO nanoparticles. *J. Magn. Mater.* 426, 347–350. <https://doi.org/10.1016/j.jmmm.2016.10.159>.
- Gan, S., Ng, H.K., Ooi, C.W., Motala, N.O., Ismail, M.A.F., 2010. Ferric sulphate catalysed esterification of free fatty acids in waste cooking oil. *Bioresour. Technol.* 101, 7338–7343. <https://doi.org/10.1016/j.biortech.2010.04.028>.
- Georgogianni, K.G., Katsoulidis, A.P., Pomonis, P.J., Kontominas, M.G., 2009. Transesterification of soybean frying oil to biodiesel using heterogeneous catalysts. *Fuel Process. Technol.* 90, 671–676. <https://doi.org/10.1016/j.fuproc.2008.12.004>.
- Gerasimov, E.Y., Isupova, L.A., Tsybulya, S.V., 2015. Microstructural features of the La_{1-x}CaxFeO_{3-δ} solid solutions prepared via Pechini route. *Mater. Res. Bull.* 70, 291–295. <https://doi.org/10.1016/j.materresbull.2015.04.041>.
- Guldhe, A., Singh, P., Ansari, F.A., Singh, B., Bux, F., 2017. Biodiesel synthesis from microalgal lipids using tungstated zirconia as a heterogeneous acid catalyst and its comparison with homogeneous acid and enzyme catalysts. *Fuel* 187, 180–188. <https://doi.org/10.1016/j.fuel.2016.09.053>.
- Gurunathan, B., Ravi, A., 2015. Biodiesel production from waste cooking oil using copper doped zinc oxide nanocomposite as heterogeneous catalyst. *Bioresour. Technol.* 188, 124–127. <https://doi.org/10.1016/j.biortech.2015.01.012>.
- Hajalilou, A., Hashim, M., Kamari, H.M., 2015. Structure and magnetic properties of Ni_{0.64}Zn_{0.36}Fe₂O₄ nanoparticles synthesized by high-energy milling and subsequent heat treatment. *J. Mater. Sci.: Mater. Electron.* 26. <https://doi.org/10.1007/s10854-014-2597-4>.
- Hermosilla, D., Han, C., Nadagouda, M.N., Machala, L., Gascó, A., Campo, P., Dionysiou, D.D., 2020. Environmentally friendly synthesized and magnetically recoverable designed ferrite photocatalysts for wastewater treatment applications. *J. Hazard. Mater.* 381. <https://doi.org/10.1016/j.jhazmat.2019.121200>.
- Jain, S.R., Adiga, K.C., Pai Verneker, V.R., 1981. A new approach to thermochemical calculations of condensed fuel-oxidizer mixtures. *Combust. Flame.* 40, 71–79. [https://doi.org/10.1016/0010-2180\(81\)90111-5](https://doi.org/10.1016/0010-2180(81)90111-5).
- Kesavamoorthi, R., Raja, C.R., 2016. Studies on the properties of manganese substituted nickel ferrite nanoparticles. *J. Supercond. Novel Magnet.* 29, 2729–2734. <https://doi.org/10.1007/s10948-016-3792-8>.
- Khot, V.M., Salunkhe, A.B., Thorat, N.D., Phadatar, M.R., Pawar, S.H., 2013. Induction heating studies of combustion synthesized MgFe₂O₄ nanoparticles for hyperthermia applications. *J. Magn. Mater.* 332, 48–51. <https://doi.org/10.1016/j.jmmm.2012.12.010>.
- Kim, J., Jung, J.M., Lee, J., Kim, K.H., Choi, T.O., Kim, J.K., Jeon, Y.J., Kwon, E.E., 2016. Pyrogenic transformation of Nanochloropsis oceanica into fatty acid methyl esters without oil extraction for estimating total lipid content. *Bioresour. Technol.* 212, 55–61. <https://doi.org/10.1016/j.biortech.2016.04.024>.
- Klug, H.P., Alexander, L.E., 1974. X-Ray diffraction procedures: for polycrystalline and amorphous materials, 2nd Edition. <https://ui.adsabs.harvard.edu/abs/1974xjdpf.book.....>
- Kombaiah, K., Vijaya, J.J., Kennedy, L.J., Bououdina, M., Al-Najar, B., 2018. Conventional and microwave combustion synthesis of optomagnetic CuFe₂O₄ nanoparticles for hyperthermia studies. *J. Phys. Chem. Solids.* 115, 162–171. <https://doi.org/10.1016/j.jpcs.2017.12.024>.
- Kombaiah, K., Vijaya, J.J., Kennedy, L.J., Kaviyarasu, K., 2019. Catalytic studies of NiFe₂O₄ nanoparticles prepared by conventional and microwave combustion method. *Mater. Chem. Phys.* 221, 11–28. <https://doi.org/10.1016/j.matchemphys.2018.09.012>.

- Lam, M.K., Lee, K.T., Mohamed, A.R., 2010. Homogeneous, heterogeneous and enzymatic catalysis for transesterification of high free fatty acid oil (waste cooking oil) to biodiesel: A review. *Biotechnol. Adv.* 28, 500–518. <https://doi.org/10.1016/j.biotechadv.2010.03.002>.
- Lamba, N., Gupta, R., Modak, J.M., Madras, G., 2019. ZnO catalyzed transesterification of Madhuca indica oil in supercritical methanol. *Fuel* 242, 323–333. <https://doi.org/10.1016/j.fuel.2019.01.044>.
- Leal, E., Dantas, J., Dos Santos, P.T.A., Bicalho, S.M. de C.M., Kiminami, R.H.G.A., Da Silva, M.R., Costa, A.C.F.M., 2018. Effect of the surface treatment on the structural, morphological, magnetic and biological properties of MFe₂O₄ iron spinels (M = Cu, Ni Co, Mn and Fe). *Appl. Surf. Sci.* 455, 635–645. <https://doi.org/10.1016/j.apsusc.2018.06.025>.
- Lee, A.F., Bennett, J.A., Manayil, J.C., Wilson, K., 2014. Heterogeneous catalysis for sustainable biodiesel production via esterification and transesterification. *Chem. Soc. Rev.* 43, 7887–7916. <https://doi.org/10.1039/C4CS00189C>.
- Li, M., Zheng, Y., Chen, Y., Zhu, X., 2014. Biodiesel production from waste cooking oil using a heterogeneous catalyst from pyrolyzed rice husk. *Bioresour. Technol.* 154, 345–348.
- Manikandan, A., Sridhar, R., Arul, Antony S., Ramakrishna, S., 2014. A simple aloe vera plant-extracted microwave and conventional combustion synthesis: Morphological, optical, magnetic and catalytic properties of CoFe₂O₄ nanostructures. *J. Mol. Struct.* 1076, 188–200. <https://doi.org/10.1016/j.molstruc.2014.07.054>.
- Mapossa, A.B., Dantas, J., Silva, M.R., Kiminami, R.H.G.A., Costa, A.C.F.M., Daramola, M.O., 2020. Catalytic performance of NiFe₂O₄ and Ni_{0.3}Zn_{0.7}Fe₂O₄ magnetic nanoparticles during biodiesel production. *Arabian J. Chem.* 13, 4462–4476. <https://doi.org/10.1016/j.arabjc.2019.09.003>.
- Mardhiah, H.H., Ong, H.C., Masjuki, H.H., Lim, S., Lee, H.V., 2017. A review on latest developments and future prospects of heterogeneous catalyst in biodiesel production from non-edible oils. *Renew. Sustain. Energy Rev.* 67, 1225–1236. <https://doi.org/10.1016/j.rser.2016.09.036>.
- Masiero, S.S., Marcilio, N.R., Perez-Lopez, O.W., 2009. Aromatization of ethane over Mo-Fe/ZSM-5 catalysts. *Catal. Lett.* 131 (1–2), 194–202. <https://doi.org/10.1007/s10562-009-0032-x>.
- Moulton, B.J.A., Rodrigues, A.M., Sampaio, D.V., Silva, L.D., Cunha, T.R., Zanotto, E.D., Pizani, P.S., 2019. The origin of the unusual DSC peaks of supercooled barium disilicate liquid. *CrystEngComm* 21, 2768–2778. <https://doi.org/10.1039/C8CE02054J>.
- Nihore, A., Aziz, F., Oswal, N., Jain, P., Subohi, O., Gupta, N., 2019. Synthesis and characterization of copper doped nickel ferrite prepared by sol-gel method. *Mater. Today: Proc.* 18, 3651–3656. <https://doi.org/10.1016/j.matpr.2019.07.298>.
- Oprimo, P.C., Pureza, V.M.M., de Oliveira, S.C., 2017. Systematic sequencing of factorial experiments as an alternative to the random order. *Gestão Produção* 24, 108–122. <https://doi.org/10.1590/0104-530x1266-16>.
- Paiva, E.J.M., Corazza, M.L., Sierakowski, M.R., Wärnå, J., Murzin, D.Y., Wypych, F., Salmi, T., 2015. Influence of two different alcohols in the esterification of fatty acids over layered zinc stearate/palmitate. *Bioresour. Technol.* 193, 337–344. <https://doi.org/10.1016/j.biortech.2015.06.079>.
- Pradhan, G.K., Parida, K.M., 2012. Dramatic enhancement of catalytic activity over transition metal substituted hematite. *J. Ind. Eng. Chem.* 18, 1612–1619. <https://doi.org/10.1016/j.jiec.2012.02.022>.
- Rashtizadeh, E., Farzaneh, F., Talebpour, Z., 2014. Synthesis and characterization of Sr₃Al₂O₆ nanocomposite as catalyst for biodiesel production. *Bioresour. Technol.* 154, 32–37. <https://doi.org/10.1016/j.biortech.2013.12.014>.
- Rietveld, H.M., 1967. Line profiles of neutron powder-diffraction peaks for structure refinement. *Acta Crystallogr.* 22, 151–152. <https://doi.org/10.1107/S0365110X67000234>.
- Saxena, V., Sharma, S., Pandey, L.M., 2019. Fe(III) doped ZnO nano-assembly as a potential heterogeneous nano-catalyst for the production of biodiesel. *Mater. Lett.* 237, 232–235. <https://doi.org/10.1016/j.matlet.2018.11.101>.
- Silva, A., Farias, A., Costa, A., 2019. Avaliação do tratamento térmico no catalisador magnético NiO, 5ZnO, 5Fe₂O₄ e sua atividade catalítica na produção de biodiesel por transesterificação e esterificação simultânea do óleo de fritura. *Cerâmica* 65, 13–27. <https://doi.org/10.1590/0366-69132019653732408>.
- Shanmugavani, A., Kalpana, D., Selvan, R.K., 2015. Electrochemical properties of CoFe₂O₄ nanoparticles as negative and Co(OH)₂ and Co₂Fe(CN)₆ as positive electrodes for supercapacitors. *Mater. Res. Bull.* 71, 133–141. <https://doi.org/10.1016/j.materresbull.2015.04.018>.
- Shi, M., Zhang, P., Fan, M., Jiang, P., Dong, Y., 2017. Influence of crystal of Fe₂O₃ in magnetism and activity of nanoparticle CaO@Fe₂O₃ for biodiesel production. *Fuel* 197, 343–347. <https://doi.org/10.1016/j.fuel.2017.02.060>.
- Shikida, P.F.A., Bachac, J.C., 1998. Aspectos econômicos da geração de tecnologia e a utilização dos principais produtos e subprodutos da agroindústria canavieira do Brasil. *Revista de Economia e Sociologia Rural* 36, 9–30.
- Sulaiman, N.F., Wan Abu Bakar, W.A., Toemen, S., Kamal, N.M., Nadarajan, R., 2019. In depth investigation of bi-functional, Cu/Zn/γ-Al₂O₃ catalyst in biodiesel production from low-grade cooking oil: optimization using response surface methodology. *Renewable Energy* 135, 408–416. <https://doi.org/10.1016/j.renene.2018.11.111>.
- Sun, Z., Duan, X., Zhao, J., Wang, X., Jiang, Z., 2015. Homogeneous borotungstic acid and heterogeneous micellar borotungstic acid catalysts for biodiesel production by esterification of free fatty acid. *Biomass Bioenergy* 76, 31–42. <https://doi.org/10.1016/j.biombioe.2015.03.002>.
- Tang, S., Wang, L., Zhang, Y., Li, S., Tian, S., Wang, B., 2012. Study on preparation of Ca/Al/Fe₃O₄ magnetic composite solid catalyst and its application in biodiesel transesterification. *Fuel Process. Technol.* 95. <https://doi.org/10.1016/j.fuproc.2011.11.022>.
- Tatarchuk, T., Myslin, M., Mironyuk, I., Bououdina, M., Pędziwiatr, A.T., Gargula, R., Bogacz, B.F., Kurzydło, P., 2020. Synthesis, morphology, crystallite size and adsorption properties of nanostructured Mg–Zn ferrites with enhanced porous structure. *J. Alloys Compounds* 819, 152945. <https://doi.org/10.1016/j.jallcom.2019.152945>.
- Tholkappian, R., Naveen, A.N., Sumithra, S., Vishista, K., 2015. Investigation on spinel MnCo₂O₄ electrode material prepared via controlled and uncontrolled synthesis route for supercapacitor application. *J. Mater. Sci.* 50, 5833–5843. <https://doi.org/10.1007/s10853-015-9132-8>.
- Vieira, D.A., Diniz, V.C.S., Cornejo, D.R., De Melo Costa, A.C.F., Kiminami, R.H.G.A., 2014. Study of the reproducibility of Ni-Zn nanoferrite obtained by combustion reaction. *Mater. Sci. Forum.* 775–776, 415–420. <https://doi.org/10.4028/www.scientific.net/MSF.775-776.415>.
- Wang, W., Jiao, Q., Zang, C., Zhu, X., 2012. Study on the absorption properties of spinel type ferrite composite coatings in the low frequency. *Adv. Mater. Res.* 415–417, 30–34. <https://doi.org/10.4028/www.scientific.net/AMR.415-417.30>.
- Widayat, Putra, D.A., Nursafitri, I., 2019. Synthesis and catalytic evaluation of hematite (α-Fe₂O₃) magnetic nanoparticles from iron

- sand for waste cooking oil conversion to produce biodiesel through esterification-transesterification method. *IOP Conf. Ser.: Mater. Sci. Eng.* 509, 12035. <https://doi.org/10.1088/1757-899x/509/1/012035>.
- Xie, W., Zhao, L., 2014. Heterogeneous CaO–MoO₃–SBA-15 catalysts for biodiesel production from soybean oil. *Energy Convers. Manage.* 79, 34–42. <https://doi.org/10.1016/j.enconman.2013.11.041>.
- Zaharieva, K., Rives, V., Tsvetkov, M., Cherkezova-Zheleva, Z., Kunev, B., Trujillano, R., Mitov, I., Milanova, M., 2015. Preparation, characterization and application of nanosized copper ferrite photocatalysts for dye degradation under UV irradiation. *Mater. Chem. Phys.* 160, 271–278. <https://doi.org/10.1016/j.matchemphys.2015.04.036>.
- Further reading**
- Mazinani, B., Kazazi, M., Mobarhan, G., Shokouhimehr, M., 2019. The combustion synthesis of Ag-Doped MnCo₂O₄ nanoparticles for supercapacitor applications. *JOM.* 71, 1499–1506. <https://doi.org/10.1007/s11837-019-03387-x>.
- Sousa, E., Frota, C., Costa, C., Silva, G., Sampaio, D., 2019. Avaliação da Oxidação e de Parâmetros de Qualidade do Óleo de Babaçu por Espectroscopia no Infravermelho Médio com Transformada de Fourier (FTIR) e Calibração Multivariada. *Revista Virtual de Química* 11 (3). <https://doi.org/10.21577/1984-6835.20190059>.